The design, hysteresis modeling and control of a novel SMA-fishing-line actuator

Qun Chao, X, Hui, Y, Zhiyong, S, Can, X, Lina, H, MD Asadur, R and Davis, ST

http://dx.doi.org/10.1088/1361-665X/aa5b03

The Design, Hysteresis Modeling and Control of a Novel SMA-Fishing-Line Actuator

The Design, Hysteresis Modeling and Control of a Novel SMA-Fishing-Line Actuator

Chaoqun Xiang[1], Hui Yang[1], Zhiyong Sun[1], Bangcan Xue[1], Lina Hao[1,3], MD. Asadur Rahoman[1], Steve Davis[2]

[1]School of Mechanical Engineering and Automation, Northeastern University, Shenyang, Liaoning, People's Republic of China

[2]Centre for Autonomous Systems and Advanced Robotics, University of Salford, Salford, United Kingdom

[3]Corresponding author (email: haolina@me.neu.edu.cn, phone: +86-13390158387)

Abstract: Fishing line can be combined with shape memory alloy (SMA) to form novel artificial muscle actuators which have low cost, are lightweight and soft. They can be applied in bionic, wearable and rehabilitation robots, and can reduce system weight and cost, increase power-to-weight ratio and offer safer physical human-robot interaction. However, these actuators possess several disadvantages, for example fishing line based actuators possess low strength and are complex to drive, and SMA possesses a low percentage contraction and has high hysteresis. This paper presents a novel artificial actuator (known as an SMA-fishing-line) made of fishing line and SMA twisted then coiled together, which can be driven directly by an electrical voltage. Its output force can reach 2.65N at 7.4V drive voltage, and the percentage contraction at 4V driven voltage with a 3N load is 7.53%. An antagonistic bionic joint driven by the novel SMA-fishing-line actuators is presented, and based on an extended unparallel Prandtl-Ishlinskii (EUPI) model, its hysteresis behavior is established, and the error ratio of the EUPI model is determined to be 6.3%. A Joule heat model of the SMA-fishing-line is also presented, and the maximum error of the established model is 0.510mm. Based on this accurate hysteresis model, a composite PID controller consisting of PID and an integral inverse (I-I) compensator is proposed and its performance is compared with a traditional PID controller through simulations and experimentation. These results show that the composite PID controller possesses higher control precision than basic PID, and is feasible for implementation in an SMA-fishing-line driven antagonistic bionic joint.

Key words: fishing line, shape memory alloy (SMA), SMA-fishing-line, hysteresis modeling, composite PID

1. Introduction

Actuators are available in a wide range of forms and convert stored energy into useful mechanical motion which allows the actuated object to interact with the environment [1]. Traditionally mechanical design has employed a limited number of actuator technologies, they include: combustion systems, hydraulic power, pneumatic power and electric motors. Even though, traditional actuation systems have seen success in conventional robotic applications, they possess technical limitations which hinder the development of robots that can be applied to or used in rehabilitation therapy and other nontraditional robotic fields. There are other issues with traditional actuators which limit their application. Burning of fuels in combustion systems is not friendly to the environment, hydraulic system has high mass and there is difficultly sealing them which can lead to liquid leakage. Pneumatic power is generally only suited to lower precision systems and electric motors have a low power to weight ratios (typically 10-500W/Kg [2]) and the need for massive transmission systems lowers this yet further.

Robots are becoming increasingly common, and are more likely to experience close physical interaction with

humans. This means that new actuators must continue to provide controlled motion, high power to weight and volume ratios and be highly portable but they must also be safe for humans operating in close proximity. In order to achieve this, novel actuators are being developed, such as shape memory alloy wires (SMA) and fishing line actuators.

With SMA actuators, as the material is heated it causes an axial shortening, however, when the material cools it returns to its original length[3]. Despite providing high power-to-weight ratio [4], the actuator has low bandwidths due to the slow cooling of the material although this can be improved by the use of forced cooling. The percentage contraction of SMA is also small. SMA is often used in bundles [5] of parallel wires which can produce greater forces without increasing the time required for individual wires to cool.

A new polymer artificial muscle made of commercial fishing line has recently been developed, the polymer is twisted then coiled to form the so-called fishing line actuator[6]. Fishing line actuators exceed the performance of mammalian skeletal muscle to deliver millions of reversible contractions of over 20%, this is considerably higher than SMA is able to achieve. The other benefits of fishing line actuators is low material cost and hysteresis which is much smaller than for SMA[6-11]. Fishing line actuators have been used as novel actuators in a range of applications [12-14].

However, the strength of fishing line actuators is low, and they can be damaged easily when in use. Zhang et al [15] used a syntactic foam composite to reinforce the fishing line artificial muscle; however, the method is highly complicated due to the fabrication process, which is not suitable for practical application. Furthermore, another disadvantage of fishing line actuators is that they can't be driven directly through the application of a voltage because a fishing line is not an electrical conductor. Instead these actuators are driven by exposure to hot and cool water or hot and cool air which changes the temperature of fishing line [6]. The work presented in this paper proposes a novel actuator made of a composite of SMA and fishing line (SMA-fishing-line). The strength of the new actuator is higher compared with the fishing line based muscles and the stroke is much larger compared to SMA actuators under the same conditions. Additionally the new actuator can be heated directly via application of a drive voltage making it easier to control than a basic fishing line actuator.

From the view of bionics, almost every single joint in a human is actuated by an agonist muscle and an antagonist muscle, e.g. the elbow joint and ankle joint[16]. When the joint is moving, the agonist muscle produces a contraction force while the antagonist muscle produces a resistance. Antagonistic joints can generate movement by adjusting the output force of both muscles. Using the novel SMA-fishing-line actuator antagonistically reduces the requirement to wait for the actuator to cool as extension of the actuator is caused by contraction of the antagonist.

The novel SMA-fishing-line actuator possesses relatively high hysteresis characteristics compared to a basic fishing line actuator. In order to precisely control an antagonistic bionic joint actuated by SMA-fishing-lines this hysteresis should be compensated for sufficiently. Due to friction in the internal structure of their materials hysteresis problems exists widely in artificial muscle actuators. The hysteresis problem in artificial muscle actuators has been well studied, and there are mainly two kinds of hysteresis modeling approaches: physical mechanism based and phenomenon based approaches. Phenomenon based approaches have attracted most researchers' attention, due to the rapid development of computer technology. Phenomenon based approaches mainly includes BW (Bouc-Wen) models, PI (Prandtl-Ishlinskii) models, Preisach models and polynomial approximation models[17]. The Preisach model is a generalized hysteresis phenomenon model, which can give a comprehensive description of a hysteresis characteristic [18], however, it needs many operators. Most hysteresis modeling methods describe symmetric hysteresis behaviors, which are relatively simple, however, they can't describe asymmetric hysteresis behavior comprehensively. Even though advanced hysteresis models have been employed in [19-20], they still cannot represent complex hysteresis precisely [21]. The hysteresis characteristic of all actuators is in fact asymmetric with the difference being in the asymmetrical level [22-23]. Song et al [24] used a BW model to characterize asymmetric hysteresis by adjusting the symmetry of the model and a modified version

of the traditional P-I model is presented in [25-26]. In [27], an extended unparallel P-I model (EUPI) is proposed, which is shown to be more flexible.

This paper proposes, for the first time, a novel SMA-fishing-line actuator which is a composite made of both SMA and fishing line. In comparison with SMA, the stroke of the SMA-fishing-line actuator is found to be higher. The output force of the SMA-fishing-line actuator is also higher than for a basic fishing line actuator. The new actuator can be driven directly by voltage making it easier to control than a basic fishing line actuator. A hysteresis model of an antagonistic bionic joint driven by SMA-fishing-lines is established through EUPI, and based on this accurate hysteresis mosdel a composite PID controller is proposed. In addition the paper proposes a Joule heat model of the SMA-fishing-line actuator. Through simulation and experimental verification the composite PID controller is shown to have better control results than a traditional PID controller.

In the first section of the paper, the novel artificial muscle (SMA-fishing-line) is described and its performance is investigated. In the second section, an antagonistic bionic joint driven by two SMA-fishing-lines is presented and its hysteresis characteristic are established. In the third section, based on this accurate hysteresis model, a composite PID controller is designed and assessed.

2. SMA-fishing-line

The novel SMA-fishing-line actuator, is made of shape memory alloy wires (SMA) and commercial fishing line. Commercial fishing line is made from high-strength polymer fibers, is readily available, inexpensive and operates up to 120℃. SMA is made from NiTi alloy, which is twisted with the fishing line then coiled together to form the SMA-fishing-line actuator. The new actuator has been designed in order to possess both the advantages of SMA and fishing line based actuators and attempt to conquer their disadvantages.

2.1 Fabrication

The fabrication process is relatively simple. A schematic diagram of the fabrication setup is shown in figure 1, it consists of a fixed support, rotary motor, a counterweight, SMA wire (black) and fishing line (green). The SMA and fishing line are straight filaments before they are fabricated, whose original diameters are 0.14mm and 0.52mm respectively. The ends of the SMA and fishing line are tied onto a hook mounted to the shaft of the rotary motor. The rotary motor applies torque to twist the SMA and fishing line, and the counterweight ensures the muscle remains vertical during construction. The counterweight is very important and should neither be too heavy nor too light. If too light, fibers of the muscle will be coiled incorrectly and if it is too heavy fibers will be broken. Angular speed of the rotary motor is also very important, if too fast, it will break the muscle. Through trial and errors, the suitable counterweight and angular speed were found to be 460g and 2022 rad/min respectively. The completed SMA-fishing-line actuator is shown in Figure 2, the green coiled material is the fishing line and the black coiled material is SMA. The diameter of this SMA-fishing-line is 1.5 mm, its length is 100mm, and its electrical resistance is 38ohms.

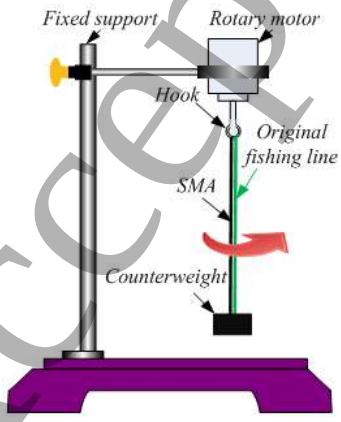

Figure 1 Schematic diagram of fabrication setup

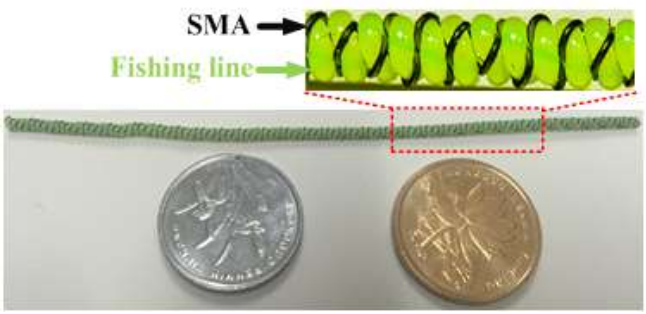

Figure 2 SMA-fishing-line

2.2 Output force test

To verify the output force characteristic of the SMA-fishing-line actuator, the total length was kept constant and the relationship between output force and drive voltage was determined experimentally. In order to compare the output force of the basic fishing line actuator and the new SMA-fishing-line actuator they were both tested in the same conditions. This meant a basic fishing line actuator needed to be fabricated which is heated by SMA, however, in this actuator the SMA only provides heat to the fishing line, it does not contribute to the force generated by the actuator. The fishing line actuator heated by SMA is shown in figure 3, the SMA is located in the middle of the coiled fishing line to make sure that it is heated evenly.

The experimental set-up diagram and the test results achieved are shown in figure 4(a) and figure 4(b) respectively. The hardware used to measure the actuator's output force consisted of a sample actuator (Diameter:1.5mm, length:100mm), a control board connected to a drive circuit whose output connects to and provides power to the actuator and a dynamometer for collecting tensile force data generated by the actuator. During experiments the drive voltage was gradually increased, the length of the muscle remained unchanged and output force was recorded through the dynamometer. The maximum voltage in use for this test was 7.4V in order not to make the temperature of SMA-fishing-line too high which would lead to its failure. Firstly the SMA-fishing-line actuator was tested, and the applied voltage spanned from 2.4V to 7.4V, with increasing increments of 0.5V. The same test was then performed on the basic fishing line actuator. The isometric test results are shown in figure 4(b).

(a)

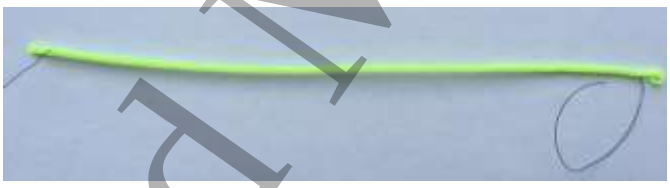

(b)

Figure 3 Fishing line with SMA (a) structure diagram, (b) physical diagram

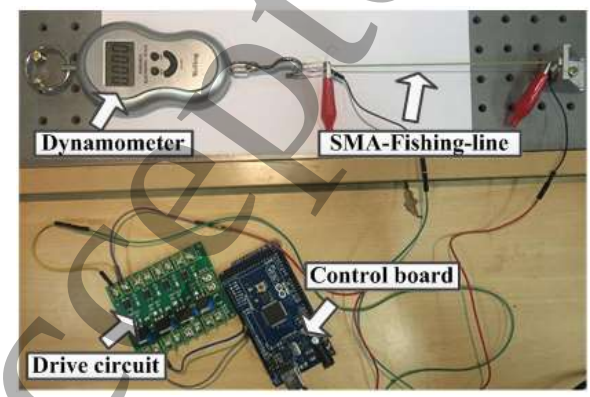

(a)

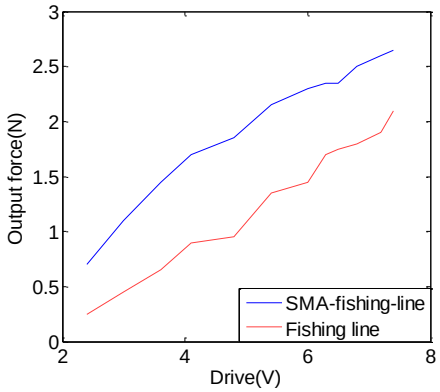

(b)

Figure 4 Relationship of output force-driving voltage test (a) experiment set-up (b) test results

2.3 Load and displacement of SMA-fishing-line

The load and displacement of the SMA-fishing-line actuator under different drive voltages is presented in the following section. The experimental set-up diagram and test results diagram are shown in figure 5(a) and (b) respectively. The experimental system consisted of a single actuator, a OADM2016441/S14F Laser sensor made by Baumer, a control unit and a series of weights. During experimentation, a set of weights of increasing magnitude were attached to the end of the SMA-fishing-line actuator. The set of weights spans from 0.05Kg to 0.3Kg, with an increment of 0.05Kg. In the experiment the drive voltage for the SMA-fishing-line actuator spans from 0V to 4V, with an increment of 2V. Each subset was repeated five times, and mean values were calculated.

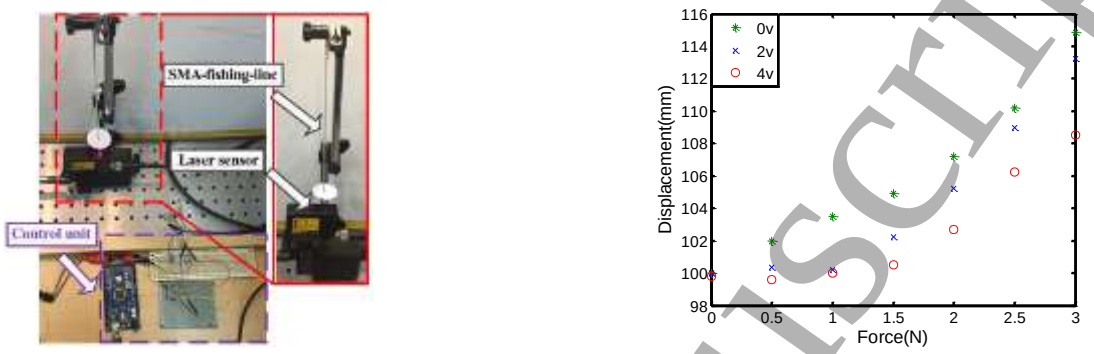

(a) (b)

Figure 5 Relationship of output displacement-driving voltage test (a) devices (b) test results

From figure 4(b), for a drive voltage of 7.4V the output force of the SMA-fishing-line actuator reached 2.65N. For isometric testing this is higher than for the basic fishing line actuator which produced just 2.1N. From figure 5(b), the maximum percentage contraction for the SMA-fishing-line actuator under 4V and a 3N load can be seen to be 7.53%. Testing of the basic fishing line actuator under the same conditions resulted in a measured contraction of just 4% [5]. Thus, the overall performance of SMA-fishing-line actuator is improved in contrast with both SMA actuators and basic fishing line actuators.

3. Hysteresis Modeling and Analysis of Antagonistic Bionic Joint Driven by SMA-fishing-lines

In contrast with a traditional motor drive systems, an antagonistic structure is relatively simple and highly flexible. This structure allows actuators which provide just a contractile force to drive a joint in both flexion and extension. This however, requires that each joint be driven by two actuators. The use of two actuators amplifies the effect of any hysteresis and to investigate this an antagonistic bionic joint driven by SMA-fishing-lines was designed as shown in figure 6. The original length of each SMA-fishing-line actuator is 100mm. For simplicity, only one SMA-fishing-line is actuated in this experiment and the other acts like a spring, the maximum displacement of the end of the link that can be achieved is 6mm.

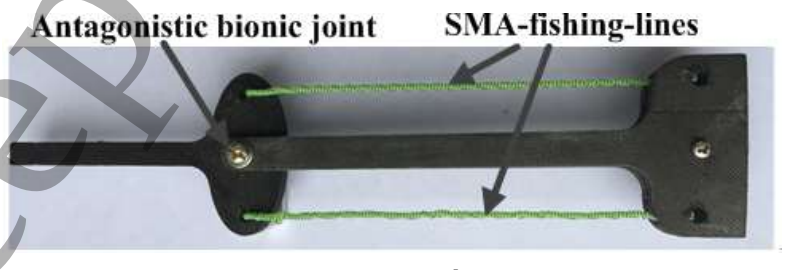

Figure 6 Antagonistic bionic joint

The hysteresis of this structure was determined by analyzing the displacement of the actuator as the driving voltage was varied. In this section, the hysteresis characteristic of the actuator is obtained experimentally and then a flexible hysteresis model using EUPI is presented.

3.1 Hysteresis characteristic experiment

The experimental test rig used, is shown in figure 7, it consisted of one antagonistic bionic joint, a laser displacement sensor, an NI DAQ card (PCI 6221 16-bit A/D converter) connecting to MATLAB to collect position data and the drive circuit connecting with output of NI DAQ card to supply the control signals to the actuator. The two signals shown in figure 8 were applied to the antagonistic SMA-fishing-line actuator system (as shown in figure 6), respectively, the input-output relations of the system was obtained and is shown in figure 9. Only positive voltages were applied to the SMA-fishing-line. The experiment is performed under quasi-static conditions.

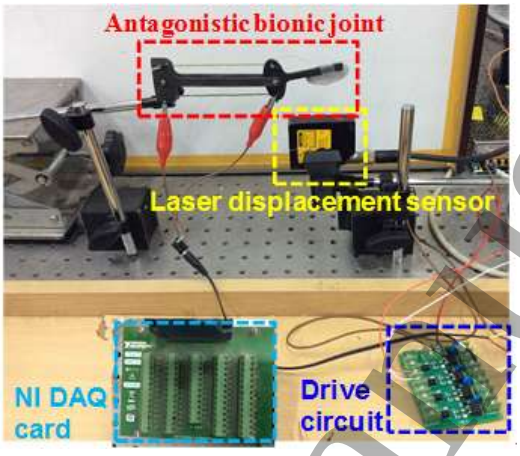

Figure 7 Hysteresis characteristic experiment test rig

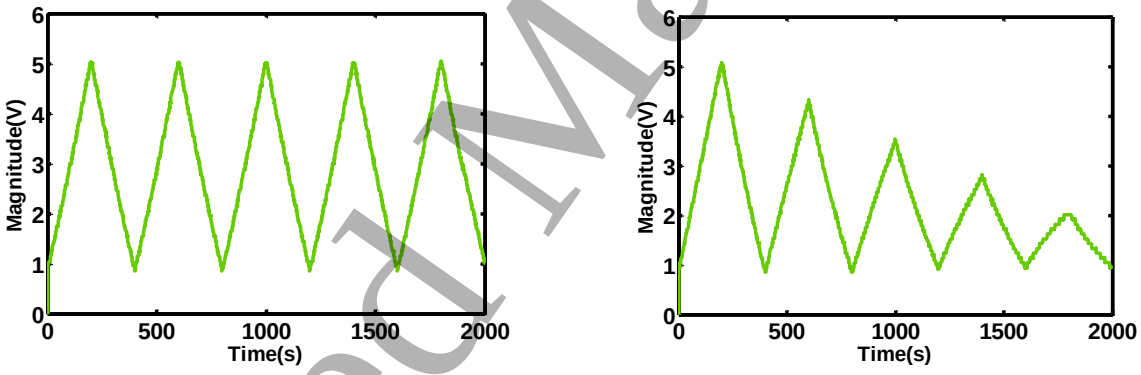

(a) (b)

Figure 8 Drive signal in the time domain (a) main loop (b) minor loop

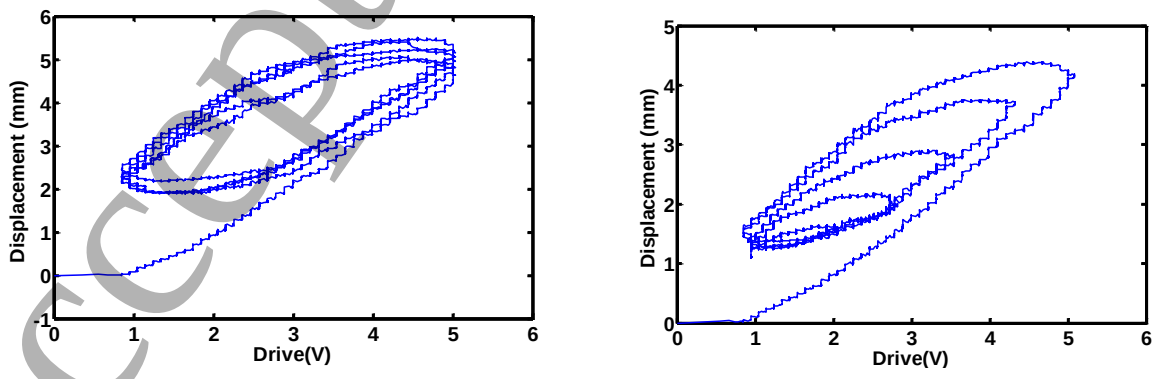

(a) (b)

Figure 9 Hysteresis phenomenon in the input-output domain (a) main loop (b) minor loop

Figure 9 (a) and (b) show the hysteresis curves under the corresponding drive signal of figure 8 (a) and (b) respectively. It shows that the hysteresis of the SMA-fishing-line actuator is very obvious. In the work of Haines et al [6] the hysteresis of the basic fishing line actuator was not obvious, however, SMA possesses a more serious hysteresis, and thus, it can be deduced that the hysteresis observed in the new actuator is mainly caused by the SMA and the friction between the fishing line and SMA. To allow the new actuator to be controllable it is vital that an accurate hysteresis model be developed.

3.2 Hysteresis modeling

The Preisach model is universal for describing hysteretic phenomena [28], but it sometimes needs a large amount of operators, such as in [29], which need more than ten thousand operators to achieve a satisfactory approximation. As an alternative, a classical PI model was developed and has been widely adopted for its convenient description and efficiency [30], however, symmetric descriptions are not suitable where hysteresis behavior is complex [31].

In order to describe the hysteresis characteristic of an antagonistic bionic joint driven by SMA-fishing-lines, a hysteresis model is established which is based on the literature [27] and which can describe a large range of asymmetric hysteresis phenomena. The model is described in (1), and is based on the UPI model and the descending edge is tilted by multiplying by a factor α_j.

$$F_{r_i,\alpha_j}[u](t) = \max\left\{u(t) - r_i, \min\{\alpha_j(u(t) + r_i), F_{r_i,\alpha_j}(t^-)\}\right\} \tag{1}$$

where r_i is the diameter of the i^{th} dead zone; α_j is the j^{th} angle edge tilt coefficient; $u(t)$ represents the drive signal at time t; $F_{r_i,\alpha_j}[u](t)$ is the UPI operator output. When α_j=1, the UPI operator can be changed into the CPI operator. From literature [32], a three-order polynomial can describe the hysteresis effectively, so the EUPI model can be expressed in (2) as follows:

$$\begin{cases} H[u](k) = \Gamma_{CPI}[u](k) + \Gamma_{UPI}[u](k) + \mathrm{P}[u](k) \\ \Gamma_{CPI}[u](k) = Gu(k) + \sum_{i=1}^{Nh} v_i F_{rj,\alpha i}[u](k) \\ \Gamma_{UPI}[u](k) = \sum_{i=1}^{Na}\sum_{j=1}^{Nr} w_{ij} F_{rj,\alpha i}[u](k) \\ \mathrm{P}[u](k) = \sum_{i=2}^{Np} x_i u^i(k) + p_0 \end{cases} \tag{2}$$

Where $\Gamma_{CPI}[u](k)$ and $\Gamma_{UPI}[u](k)$ represents the CPI symmetric portion and UPI asymmetric portion respectively; $\mathrm{P}[u](k)$ is the polynomial portion; N_r *and* N_a are the number of the dead zones; p_0 is an offset associated with the hysteresis loops working range. G is for amplifying the input, $u(k)$. v_i, w_{ij} and x_i are gains in accordance with the CPI, UPI and polynomial operators respectively. The estimation procedures were conducted utilizing a constrained least squares method, and the identification results and modeling error are shown in figure 10(a) and figure 10(b) respectively.

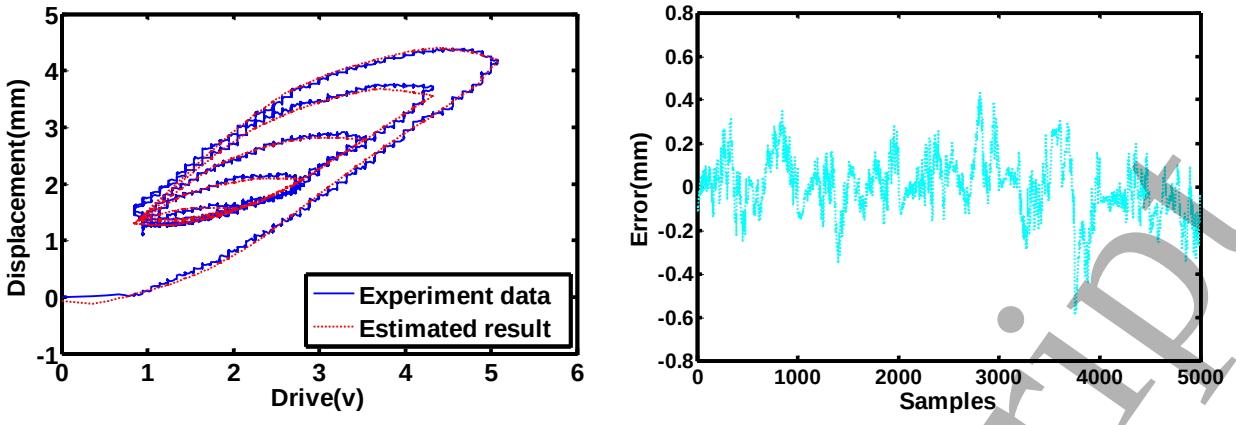

(a) (b)

Figure 10 Hysteresis modeling (a) input-output relationship modeling using EUPI model, (b) modeling error

From figure 10, the hysteresis of the antagonistic bionic joint driven by SMA-fishing-lines can be described by the EUPI model. In order to investigate the modeling accuracy, the following equation is expressed in (3) as follow,

$$e_r = \frac{e_{\max}}{W_r} \times 100\% \tag{3}$$

where e_r is the error ratio of the model; $e_{\max}$ is the maxim error on the whole work range; *Wr* respects the whole work range. After calculation, the error ratio of the EUPI model was determined to be 6.3%, which indicates the modeling performance which can be described using the EUPI modeling method.

3.3 Joule heat model of SMA-fishing-line

For the new SMA-fishing-line actuator, all the heat required to contract the fishing line comes from the application of an electrical current to the SMA wire. Assuming J(t) is the heat produced by the SMA, and the surrounding environmental temperature is T_0, then the temperature of the SMA-fishing-line actuator T(t) is expressed as follows,

$$\begin{aligned} &\frac{dT}{dt} = K_1(T_0 - T) + K_2 J(t), \quad \text{s.t. } K_1, K_2 > 0 \\ &J(t) = \frac{U^2(t)}{R_{\text{SMA}}} \end{aligned} \tag{4}$$

where K_1, K_2 are positive model parameters, which are identified through experimentation; R_{SMA} is the electrical resistance of the SMA, which was measured and found to be 38ohm. When the voltage applied to the SMA-fishing-line actuator is controlled so its temperature is varied. So taking $U_2(t)$ as the input, equation (4) can be modified as follows (5).

$$\begin{aligned} &\frac{dT(t)}{dt} + K_1 T(t) = M(t), \quad \text{s.t. } K_1, K_2 > 0 \\ &M(t) = K_1 T_0 + \frac{K_2}{R_{\text{SMA}}} U^2(t) = \frac{K_2}{R_{\text{SMA}}} (U^2(t) + \frac{K_1 T_0 R_{\text{SMA}}}{K_2}) \end{aligned} \tag{5}$$

Using Laplace transforms, (5) can be expressed as (6),

$$\frac{T(s)}{M(s)} = \frac{1}{1 + K_1 s} \tag{6}$$

Using the experimental test rig shown in figure 7 a driving voltage was applied to the SMA-fishing-line and

input voltage vs displacement data was obtained, as seen in figure 11.

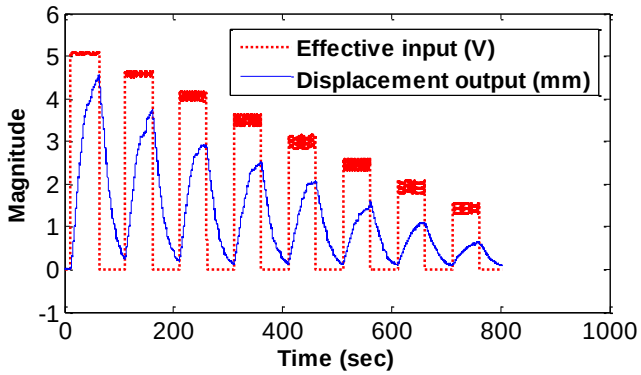

Figure 11 Effective input voltage and displacement of SMA-fishing-line

Equation (6) is used to model of SMA-fishing-line actuator and the modelled data and practically obtained experimental results are both shown in figure 12. The Joule heat model of the SMA-fishing-line actuator is shown in equation (7).

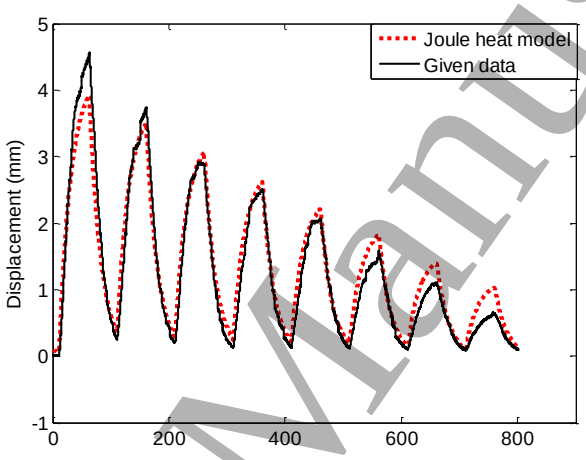

Figure 12 Modeling result

$$\frac{T(s)}{M'(s)} = \frac{0.04172}{s + 0.04988} \Rightarrow \begin{cases} K1 = 0.04988 \\ K2 = 0.04172 \end{cases} \quad (7)$$

From figure 12 it can be seen that that modelled data matches the experimental data with a reasonable degree of accuracy, the maximum error for the Joule heat model was determined to be 0.510mm. Therefore equation (6) can reliably be used to characterize the behavior of the new SMA-fishing-line actuator.

4. Inverse compensators controller design and experiment verification

A hysteresis inverse compensation control strategy can decrease or eliminate the influence of hysteresis characteristics. Most of the inverse compensation controllers are designed based on an inverse model of the hysteresis behavior [33]. For the integral inverse (I-I) scheme, inverse compensation controllers can easily be obtained through the production of a forward model. Based on this a hysteresis compensator has been designed using an integral inverse (I-I) compensation strategy, this has been combined with a PID control strategy allowing a closed-loop control scheme for the SMA-fishing-line actuator to be implemented. In order to verify the hysteresis compensation effect, closed loop control tests of the SMA-fishing-line actuator were performed.

4.1 Inverse compensators controller design

In order to make good use of the accurate hysteresis model, a composite PID controller was designed, which consisted of a PID and I-I compensator. The I-I compensator is adjusted by modifying the integral, which contains a tunable parameter of the inverse scheme, *K*, and an integrator *ƒ*. *K* should be neither too high nor too low, if too high this will lead to high amounts of overshoot, if too low it will affect the compensation effect [29]. The optimal value of *K* is selected through experimentation. The control block diagram is shown in figure 13 and allows an antagonistic bionic joint driven by SMA-fishing-lines to be controlled using composite PID. As seen in figure 13, the output of the I-I compensator $u_{2(t)}$ is added to the output signal of the PID controller $u_{1(t)}$ to form the input drive voltage signal $u_{3(t)}$.

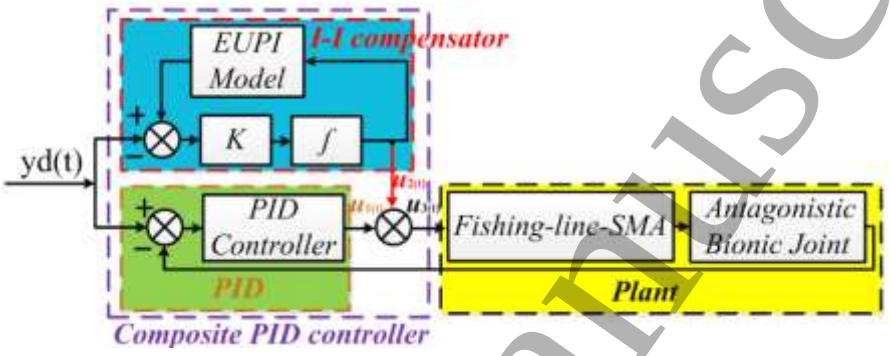

Figure 13 Control block diagram of composite PID

4.2 Composite PID controller simulation analysis

To investigate the control effect of the composite PID controller, a PID controller and composite PID controller were applied to control a simulated antagonistic bionic joint for the purpose of comparison. The Joule heat model of the SMA-fishing-line actuator was used to model the actuator and MATLAB was used to perform the simulations. A sine signal $\sin(3\pi/10*t+\pi/2)+1.5$ and a step signal of 2.5 amplitude were applied as the reference signal, respectively. Through Ziegler-Nichols theorem, the control parameters of the PID and composite PID were adjusted, and the optimum values were found to be the same in both instances, namely, proportion equal to 35, integral equal to 20, and derivative equal to 0. The tunable parameter of the inverse scheme, *K*, was set 10. The simulation results for the sine signal are shown in figure 14(a) and (b) and figure 15(a) and (b) show the simulation results for the step signal.

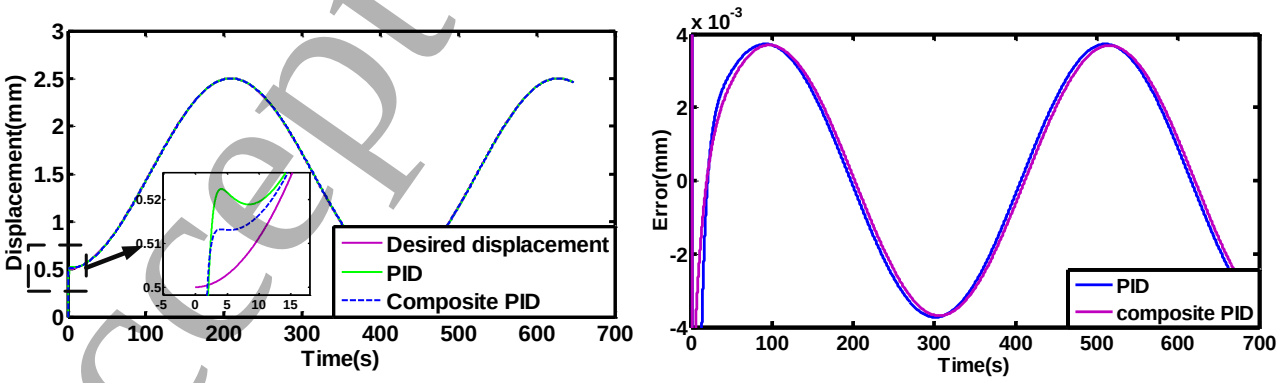

(a) tracking results (b) tracking errors

Figure 14 Simulation results of tracking sine signal (a) tracking result, (b) tracking errors

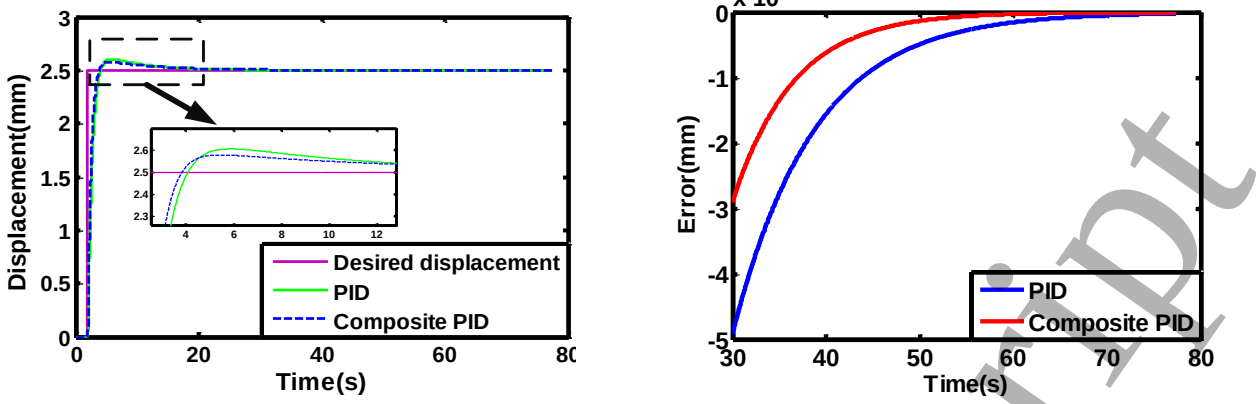

(a) tracking results (b) steady errors

Figure 15 Simulation results of tracking step signal (a) tracking result, (b) steady error

From figure14 and 15 it can be seen that the control effect of the composite PID is better than for the traditional PID controller. In order to further compare these two controllers, a criterion used for evaluating the overall control accuracy was introduced using the following function:

$$e_{mean} = \frac{\sum_{k=1}^{N} | y_d(k) - y(k) |}{N} \tag{8}$$

where e_{mean} is the mean error ratio of the model; $y_d(k)$ and $y(k)$ are the desired displacement and actual output displacement at time k, respectively and N is the total sample time number. After calculation the value of e_{mean} for the composite PID when tracking the sine signal and step signal was 0.0027mm and 0.0004mm, respectively, while for the PID controller the values were 0.0030mm and 0.0009mm, respectively. This proves that the composite PID controller shows higher control precision than PID.

4.3 Experiment verification

To experimentally test the controller the same experimental rig (figure 7) used in the rest of the paper was again used and the control block diagram was as shown in figure 13. The control parameters of the PID and composite PID controllers were adjusted and their optimum values were determined to be; proportion equal to 30, integral equal to 30, and derivative equal to 0. The tunable parameter of the inverse scheme, K, was set 10. The experimental results for the sine input signal are shown in figure 16(a) and (b) respectively and figure 17(a) and (b) show the experimental results for the step input signal.

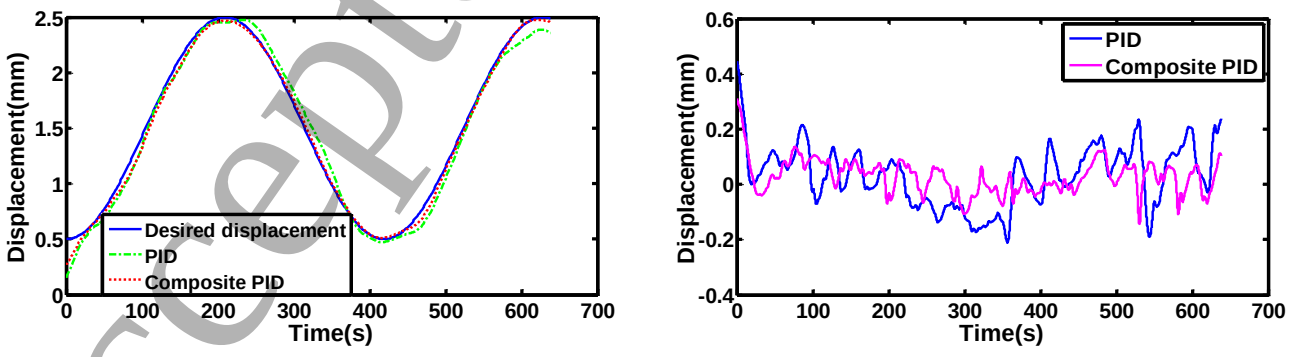

(a) tracking results (b) tracking errors

Figure 16 Experiment results of tracking sine signal (a) tracking result, (b) tracking errors

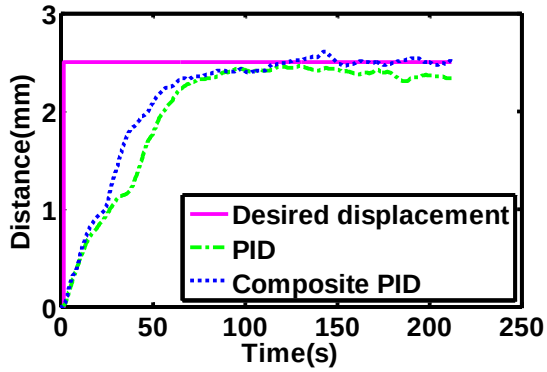

(a) tracking results

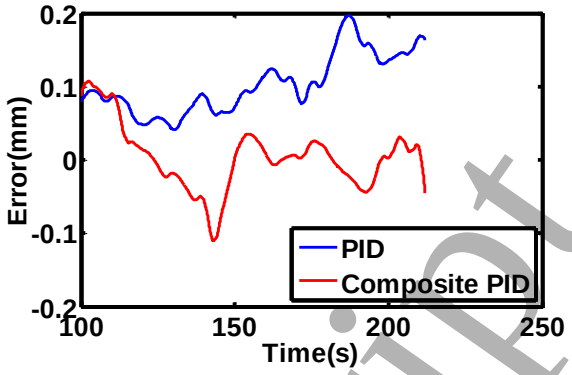

(b) steady errors

Figure 17 Experiment results of tracking step signal (a) tracking result, (b) steady error

From figure 16 and 17, the experimental results also show the enhanced perfromance of the composite PID controller when compared to the traditional PID controller. Using (8), e_{mean} of the composite PID when tracking a sine signal and a step signal were found to be 0.0517mm and 0.0326mm respectively. For the basic PID controller e_{mean} was found to be 0.0934mm and 0.1029mm for the sine and step inputs respectively. This proves that the composite PID achieves greater control precision than basic PID. Thus based on an accurate hysteresis model an I-I compensator possesses prediction abilities, namely, it can predict the future movement of the system. However, it was found that for the composite PID tracking a sine signal the controller was less effective than when tracking a step signal. This means that the I-I compensator is suitable to compensate a low frequency signal, due to the static characteristic of the hysteresis.

5. Conclusion

Fishing line and SMA artificial muscle actuators have many advantages, such as low cost, and low weight. However, they also possess many disadvantages, such as low strength, complexity in driving them, low percentage contraction, and high level of hysteresis. In this research, a novel artificial actuator is presented. The SMA-fishing-line actuator proposed in this paper, is made of fishing line and SMA twisted then coiled together. Due to the inherent electrical heating characteristic of the SMA, it can be driven directly by voltage (basic fishing line actuators need to be heated by an external source) which is convenient for control. The stroke of the SMA-fishing-line actuator is improved by a factor of nearly two when compared with SMA actuators. Additionally the output force of the SMA-fishing-line actuator has been shown to be higher than a basic fishing line actuator.

An antagonistic bionic joint driven by SMA-fishing-lines has been designed, and based on a flexible hysteresis modeling method, EUPI model, its hysteresis model was established. A Joule heat model of the SMA-fishing-line actuator was established, and the maximum error was determined to be 0.510mm. Based on this accurate hysteresis model a composite PID controller has been designed, which consists of PID and an I-I compensator. The effectiveness of the controller has been determined both practically and in simulation. In both cases the composite PID was shown to provide higher control precision than a conventional PID controller thus composite PID is more suitable for implementation in a SMA-fishing-line driven antagonistic bionic joint.

Acknowledgments

This work was particularly supported by the National High Technology Research, Development Program of China (863 program) under Grant No. 2015AA042302, NSFC under grant 61573093, the Fundamental Research Funds for the Central Universities of China under grant N150308001, and the Equipment Pre-Research Program of China under Grant No. 62501040412. The authors would also like to sincerely thank the reviewers and editors for their very pertinent remarks that helped this article become clearer and more precise.

Reference

1. D.G. Caldwell, N. Tsagarakis, G.A. Medrano-Cerda. "Bio-mimetic Actuators: Polymeric Pseudo Muscular Actuators for Biological Emulation". Mechatronics. 2000.
2. ESCAP Motion Systems. Product Catalogue.
3. Shu S G, Lagoudas D C, Hughes D, et al. Modeling of a flexible beam actuated by shape memory alloy wires[J]. Smart Materials and Structures, 1997, 6(3): 265.
4. D. Grant, V. Hayward. "Constrained Force Control of Shape Memory Alloy Actuators". International Conference on Robotics and Automation. San Francisco, CA, USA. April 2000.
5. K.J. De Laurentis , A. Fisch, J. Nikitczuk, C. Mavroidis. "Optimal Design of Shape Memory Alloy Wire Bundle Actuators". International Conference on Robotics and Automation. Washington, USA. May 2002.
6. Haines C S, Lima M D, Li N, et al. Artificial muscles from fishing line and sewing thread[J]. science, 2014, 343(6173): 868-872.
7. Zhang P, Li G. Healing-on-demand composites based on polymer artificial muscle[J]. Polymer, 2015, 64: 29-38.
8. Sharafi S, Li G. A multiscale approach for modeling actuation response of polymeric artificial muscles[J]. Soft matter, 2015, 11(19): 3833-3843.
9. Aziz S, Naficy S, Foroughi J, et al. Characterisation of torsional actuation in highly twisted yarns and fibres[J]. Polymer Testing, 2015, 46: 88-97.
10. Madden J D W, Kianzad S. Twisted lines: artificial muscle and advanced instruments can be formed from nylon threads and fabric[J]. Pulse, IEEE, 2015, 6(1): 32-35.
11. Mirvakili S M, Ravandi A R, Hunter I W, et al. Simple and strong: Twisted silver painted nylon artificial muscle actuated by Joule heating[C]//SPIE Smart Structures and Materials+ Nondestructive Evaluation and Health Monitoring. International Society for Optics and Photonics, 2014: 90560I-90560I-10.
12. Wu L, de Andrade M J, Rome R S, et al. Nylon-muscle-actuated robotic finger[C]//SPIE Smart Structures and Materials+ Nondestructive Evaluation and Health Monitoring. International Society for Optics and Photonics, 2015: 94310I-94310I-12.
13. Wu L, de Andrade M J, Brahme T, et al. A deformable robot with tensegrity structure using nylon artificial muscle[C]//SPIE Smart Structures and Materials+ Nondestructive Evaluation and Health Monitoring. International Society for Optics and Photonics, 2016: 97993K-97993K-12.
14. Cho K H, Song M G, Jung H, et al. A robotic finger driven by twisted and coiled polymer actuator[C]//SPIE Smart Structures and Materials+ Nondestructive Evaluation and Health Monitoring. International Society for Optics and Photonics, 2016: 97981J-97981J-7.
15. Zhang P, Li G. Fishing line artificial muscle reinforced composite for impact mitigation and on-demand damage healing[J]. Journal of Composite Materials, 2016: 0021998316636454.
16. Marieb E N, Hoehn K. Human anatomy & physiology[M]. Pearson Education, 2007.
17. Hassani V, Tjahjowidodo T, Do T N. A survey on hysteresis modeling, identification and control[J]. Mechanical systems and signal processing, 2014, 49(1): 209-233.
18. Zhang J, Merced E, Sepúlveda N, et al. Modeling and Inverse Compensation of Nonmonotonic Hysteresis in VO-Coated Microactuators[J]. Mechatronics, IEEE/ASME Transactions on, 2014, 19(2): 579-588.
19. A. Esbrook, X. Tan, and H. K. Khalil, "Control of systems with hysteresis via servocompensation and its application to nanopositioning," Control Systems Technology, IEEE Transactions on, vol. 21, no. 3, pp. 725–738, 2013.
20. A. Esbrook, X. Tan, and H. K. Khalil, "Inversion-free stabilization and regulation of systems with hysteresis via integral action," Automatica, vol. 50, no. 4, pp. 1017–1025, 2014.

21. K. Kuhnen, "Modeling, identification and compensation of complex hysteretic nonlinearities: A modified prandtl-ishlinskii approach," European journal of control, vol. 9, no. 4, pp. 407–418, 2003.
22. Li Y, Xu Q. Adaptive sliding mode control with perturbation estimation and PID sliding surface for motion tracking of a piezo-driven micromanipulator[J]. Control Systems Technology, IEEE Transactions on, 2010, 18(4): 798-810.
23. P.-L. Yen, M.-T. Yan, and Y. Chen, "Hysteresis compensation and adaptive controller design for a piezoceramic actuat or system in atomic force microscopy," Asian Journal of Control, vol. 14, no. 4, pp. 1012–1027, 2012.
24. J.Song, and A.D.Kiureghian: 'Generalized Bouc-Wen model for highly asymmetric hysteresis', J.Eng.Mech, 2006, 132(6): 610-618.
25. S. Liu, and C.-Y. Su: 'A note on the properties of a generalized Prandtl–Ishlinskii model', SMART MATERIALS AND STRUCTURES, 2011, 20: 087003.
26. H. Jiang, H.-L.Ji, J.-H.Qiu, Y.-S. Chen: 'A modified Prandtl-Ishlinskii model for modeling asymmetric hysteresis of piezoelectric actuators' , IEEE Trans Ultras on Ferroelectr Freq Control, 2010, 57(5): 1200-1210.
27. Sun Z, Song B, Xi N, et al. Compensating asymmetric hysteresis for nanorobot motion control[C]//Robotics and Automation (ICRA), 2015 IEEE International Conference on. IEEE, 2015: 3501-3506.
28. K. Kuhnen and P. Krejci, "Compensation of complex hysteresis and creep effects in piezoelectrically actuated systemsła new preisach modeling approach," Automatic Control, IEEE Transactions on, vol. 54, no. 3, pp. 537–550, 2009.
29. Li Z, Su C Y, Chai T. Compensation of hysteresis nonlinearity in magnetostrictive actuators with inverse multiplicative structure for Preisach model[J]. Automation Science and Engineering, IEEE Transactions on, 2014, 11(2): 613-619.
30. P. Krejci and K. Kuhnen, "Inverse control of systems with hysteresis and creep," IEE Proceedings-Control Theory and Applications, vol. 148, no. 3, pp. 185–192, 2001
31. M. Al Janaideh, S. Rakheja, and C.-Y. Su, "An analytical generalized prandtl–ishlinskii model inversion for hysteresis compensation in micropositioning control," Mechatronics, IEEE/ASME Transactions on, vol. 16, no. 4, pp. 734–744, 2011.
32. S. Bashash, and N. Jalili: 'A polynomial-based linear mapping strategy for feed-forward compensation of hysteresis in piezoelectric actuators', Journal of Dynamic System, Measurement and Control, 2008, 130(3): 031008.
33. K.Kuhnen, and H.Janocha: 'Inverse feed forward controller for complex hysteretic nonlinearities in smart-material systems', Control and Intelligent systems, 2001, 29(3): 74-83.